



BACHELOR THESIS

Precision computation of phase boundaries of QCD-inspired models in the large-N limit

Author:
Jonas STOLL

Supervisor and 1. Examiner:
Professor Doktor WAGNER

2. Examiner:
Professor Doktor RISCHKE

Echzell, October 22, 2019

Declaration of Authorship

I, Jonas STOLL, declare that this thesis titled, “Precision computation of phase boundaries of QCD-inspired models in the large-N limit” and the work presented in it are my own. I confirm that:

- No part has previously been submitted for any other qualification
- Where I have consulted the work of others, this is attributed
- I have acknowledged all main sources of help.

Signed:

Date:

GOETHE UNIVERSITY

Abstract

Institute for Theoretical Physics

Precision computation of phase boundaries of QCD-inspired models in the large-N limit

by Jonas STOLL

In this Bachelor thesis, the focus is on inhomogeneous chiral condensates at the example of the Gross Neveu model (GN) in 1+1 dimensions in the large-N limit, at finite temperature (T) and chemical potential (μ). Methods are investigated to calculate phase boundaries numerically, which should later be generalized to more complicated Quantum Chromodynamic (QCD) inspired theories. Especially the phase boundary from the inhomogeneous to homogeneous phase is investigated by a stability analysis and occurring finite volume effects are removed. Additionally, possible accelerations for the time consuming numerical eigenvalue calculation of the Hessian matrix are explored.

Contents

Declaration of Authorship	i
Abstract	ii
1 Introduction	1
2 Theoretical background and Motivation	2
3 GN model in 1+1 dimensions	5
4 Implementation	8
5 Homogeneous phase diagram	11
6 Inhomogeneous phase diagram	15
7 Computing time improvements	21
7.1 Determinants of first minors	21
7.2 Shifted matrix combined with power method	22
7.3 Eigenvalue calculation via Tridiagonalization and QR decomposition (GSL and LAPACK)	23
7.3.1 Tridiagonalization	24
7.3.2 QR decomposition	24
7.3.3 LAPACK function: zheevr	25
7.4 Run time measurement	26
8 Conclusion	28
8.1 Outlook	28
8.2 Acknowledgements	28

Chapter 1

Introduction

The topic of this bachelor thesis is put of the research programme of the CRC-TR 211 project A03. The collaborative research center investigates in strong interacting matter under extreme conditions in temperature and chemical potential, while the subordinated A03 project examines inhomogeneous phases in Quantum Chromodynamics (QCD) or QCD inspired models at low temperature and high chemical potential [5].

One of the simplest examples of a QCD like theory is the 1+1 dimensional GN model in the large N-limit. Such unphysical theories (they do not describe particles that occur in nature) are used to research low T and high μ areas, where QCD simulations did not yield results, yet [21]. The GN model [4] is, as an analytically solved QCD like theory useful to develop methods for computing a chiral phase diagram in the μ, T plane. The phases differ in the presence, absence or space dependent presence of chiral symmetry. The expectation value of a scalar field σ corresponding to the chiral condensate is used as order parameter. In the large-N limit only the global minimum of the action as a function of the field σ describes physics and therefore this minimum needs to be found to calculate expectation values like the chiral condensate [6]. A purely homogeneous phase diagram with spatially constant σ as well as a possibly space dependent σ are researched. Treating the GN model numerically, no ansatz for the shape of a chiral condensate is needed and furthermore, the results can be verified by the analytical solution [3]. To handle the infinite field degrees of freedom (dof's) numerically they are reduced by lattice discretization and/or basis function expansion. Since numerical tests and partially analytical proofs show an extremum for the action at $\sigma = 0$ in all phases, a stability analysis can be used to determine second order transitions to the homogeneous phase (global minimum of the action in $\sigma = 0$). The numerical results match up with the analytical ones relatively good, but finite volume effects at the homogeneous to inhomogeneous phase boundary disturb them. The reason is, that the wavelength of a spatially oscillating σ does not match into the finite volume, but the periodic boundary conditions force σ to adopt an inappropriate function [1]. The main emphasis of the thesis is an algorithm to remove this effects [2] and the improved results are graphically compared to the previous ones. The algorithm is slow because all eigenvalues of a large matrix are computed, although only the lowest one is needed. Four algorithms: First minors, Power Method, or library functions from GSL and LAPACK [7][16 - 20], that were candidates for speeding the computation up, are presented and compared. All of them perform on an similar level. Finally some outlook for the following goals is given.

Chapter 2

Theoretical background and Motivation

This chapter gives a brief introduction to (thermodynamical) Quantum Field Theory (QFT) [8][9] at the important example of QCD. Furthermore, the way such theories are handled numerically [10] and the reason for investigating in more or less unphysical models and their behavior [11] is described. The natural unit system and euclidean spacetime is used in the following.

In QFT, matter is represented through fields, like in quantum mechanics, but in a many-body system. Also, interaction between matter is represented through so-called gauge fields. A QFT in the path integral formalism is given by a Lagrangian or equivalent an action containing classical nonoperator fields by which one can theoretically calculate the path integral Z and thus the expectation values of variables/observables O that are dependent on the occurring fields (collected in Φ)

$$\langle O \rangle = \frac{\int D\Phi O(\Phi) \cdot e^{-S[\Phi]}}{Z} \quad \text{with} \quad Z = \int D\Phi e^{-S[\Phi]} \quad (2.1)$$

A theory, where fields (e.g. matter and gauge) are coupled to each other by multiplication is called interacting field theory. If powers of fields higher than quadratic order or field mixing terms in interacting field theories occur the path integral is usually not analytically solvable [8]. For some QFT's it is additionally not possible to expand the integral in low energies because interacting field theories with a nonabelian gauge group can lead to an effect called asymptotic freedom with a coupling constant that is big for low energies (high distances) and low for high energies (small distances). Therefore only high energy expansions and precise forecasts are possible. In practice, this is observable as an effect called confinement, that prohibits observations of single particles of these fields, because moving them away from each other leads to a growing force until the energy is enough to produce two new particles and both pairs are confined again.

QFT includes none of the thermodynamical properties like temperature or chemical potential, but it can be extend to a statistical field theory which contains these. By comparing the thermodynamical partition function with the path integral a great similarity occurs and the time t can be identified with the inverse temperature T : $t \propto \frac{1}{k_b \cdot T} = \beta$. The following operations should be understood as a rough picturing (for details see [8][9]):

$$\begin{aligned} \text{Partition function: } \sum_i e^{-\beta \cdot E_i} \quad \text{Path integral: } Z &= \int D\Phi e^{-S[\Phi]} & (2.2) \\ Z &= \int e^{-S[\Phi]} = \langle \Phi_f(t_f, \vec{x}) | \Phi_i(t_i, \vec{x}) \rangle \\ &\approx \langle \Phi_f(\vec{x}) | e^{-\Delta t H} | \Phi_i(\vec{x}) \rangle \sim \sum_i e^{-\Delta t E_i} \\ &\Rightarrow \Delta t \sim \beta \end{aligned}$$

S is the action, H is the Hamilton operator, E_i an energy eigenvalue of the system and Φ_i & Φ_f are in- and outgoing states of the field. As a result of this derivation, time expansion is finite in the following, corresponding to the inverse system temperature.

Hereinafter, fermionic Grassmann fields ψ will be treated. The chemical potential μ is inserted coupled to the zeros Dirac matrix γ_0 , since it describes the particle density ρ (i.e. if there is an excess or lack of particles).

$$\bar{\psi}\gamma_0\mu\psi = \mu\psi^\dagger\gamma_0^2\psi = \mu\psi^\dagger\psi \sim \mu\rho \quad (2.3)$$

A practical example for an asymptotically free QFT is QCD with the nonabelian gauge group $SU(3)$, that describes the strong interaction between quarks by the interaction particles called gluons. Both carry the charge color and are therefore confined at low energies, which leads to the building of indivisible hadrons like protons and neutrons. The quark sector of the QCD Lagrangian has another approximate symmetry called chirality [12]. Chiral symmetry means, that the Lagrangian is unchanged under a chiral symmetry transformation, which is the case if it can be divided into independent left- and a right-handed fermionic field parts ($\psi_{L,R}$), that describe two different type of particles [8].

$$\text{Distinction of the field: } \psi = \underbrace{\frac{1 - \gamma_5}{2} \cdot \psi}_{\psi_L} + \underbrace{\frac{1 + \gamma_5}{2} \cdot \psi}_{\psi_R} \quad (2.4)$$

γ_5 is the fifth Dirac matrix.

The chiral symmetry of QCD is explicitly broken, because QCD has a mass term for every flavor, proportional to $(\bar{\psi}\psi)^2$, which is not separable into left and right handed fields:

$$\begin{aligned} (\bar{\psi}\psi)^2 &= [(\bar{\psi}_L + \bar{\psi}_R) \cdot (\psi_R + \psi_L)]^2 \\ &= \bar{\psi}_L\psi_R\bar{\psi}_L\psi_R + \bar{\psi}_L\psi_R\bar{\psi}_R\psi_L + \bar{\psi}_R\psi_L\bar{\psi}_L\psi_R + \bar{\psi}_R\psi_L\bar{\psi}_R\psi_L \end{aligned} \quad (2.5)$$

Since the flavors up and down are very light in comparison to the other flavors, QCD is approximately chirally symmetric for these [12]. The approximate symmetry is spontaneously broken for some μ and T in thermodynamical QCD, which in simple words means that the ground state of the field has less symmetries, than its equation of motion. Therefore it can be used to calculate a chiral phase diagram. Absence, presence of the symmetry or the spatial shape of the ground state, identified with the later introduced chiral condensate, is used to indicate the different phases in the diagram.

To calculate expectation values of observables at low energies, non perturbative lattice QCD simulations can be used, since low energy expansion is impossible. To handle a field theory numerically the infinite degrees of freedom of the field need to be reduced, for example by discretizing spacetime to a lattice. Additionally, the number of lattice points needs to be finite, which is realized by creating a space time hyper torus, with periodic boundary conditions. The path integral can then be calculated explicitly (for example by Monte Carlo integration [9]). For sufficiently low lattice point distances the continuum solution of the field is reproduced [10]. This way of solving the problem is numerically very expensive and unusable for chemical potential much bigger than zero because the numerical sign problem (incalculable oscillating integrals) occurs for high densities [11].

Another way to approach the QCD phase diagram problem is to investigate effective alternative theories, which are QCD like i.e. they fulfill some similar properties than the original one, but do not bring up a sign problem or can be calculated analytically. Two of these properties are: asymptotical freedom and spontaneously chiral symmetry breaking. There are several theories that fulfill some of these properties, but one of the easiest and already analytically solved one is the GN model in 1+1 dimensions. It

is renormalizable, asymptotically free and spontaneously chiral symmetry breaking occurs. No gauge fields are part of the theory, but a four-fermion-selfinteraction. Nevertheless, there are big differences to QCD, like 2 missing spatial dimensions or the absence of gauge fields, but if different effective models produce similar phase diagrams, the assumption that the one of QCD looks also similar is at least reasonable [22]. That is why the investigation in unphysical models is worthwhile. To handle more complicated effective theories, that are also in a large- N limit, but not analytically solved, stable algorithms are needed to find phase boundaries and a solved theory (e.g. GN) is perfect to develop them.

Chapter 3

GN model in 1+1 dimensions

The GN model in 1+1 dimensions in the large-N limit is a relativistic field theory of Dirac fermions and a simple example of QCD like theories [4]. Its correct analytical solution, with an inhomogeneous phase region was found [3], after doubts came up in the 2000's whether a purely homogeneous solution ($\sigma = \text{const}$) is the stablest one. This chapter is based on the stated papers.

Starting point is a massless QFT Lagrangian with N fields ψ_f named flavors, a coupling g , the Dirac matrices γ^μ , and a quadratic selfinteraction.

$$\mathcal{L} = \sum_{f=1}^N \bar{\psi}_f \gamma^\mu \partial_\mu \psi_f + \frac{1}{2} g^2 \left(\sum_{f=1}^N \bar{\psi}_f \psi_f \right)^2 \quad (3.1)$$

1+1 dimensions are used since the theory is asymptotically free, without gauge fields in this case, which is impossible in higher dimensions. Without a mass the theory fulfills chiral symmetry. Translating the Lagrangian into a thermodynamical QFT by introducing the chemical potential $\gamma_0 \mu$ and associating time with the inverse temperature leads to the following theory:

$$\mathcal{L} = \sum_f \bar{\psi}_f (\gamma^\mu \partial_\mu - \gamma_0 \mu) \psi_f + \frac{1}{2} g^2 \left(\sum_f \bar{\psi}_f \psi_f \right)^2 \quad (3.2)$$

The chiral symmetry of this theory is spontaneously broken for certain μ and T. Since the GN model was developed to investigate it analytically, the four fermion interaction needs to be removed because the path integral can otherwise not be calculated. There are various ways to do so, like introducing a new action, which additionally depends on a scalar field σ .

$$S[\bar{\psi}, \psi] = \int d^2 X \left(\sum_f \bar{\psi}_f (\gamma_\mu \partial^\mu) \psi^f + \sum_f \bar{\psi}_f (\gamma_0 \cdot \mu) \psi^f - \frac{1}{2} g^2 \left(\sum_f \bar{\psi}_f \psi^f \right)^2 \right) \quad (3.3)$$

$$\tilde{S}[\bar{\psi}, \psi, \sigma] = \int d^2 X \left(\frac{1}{2g^2} \sigma^2 + \sum_f \bar{\psi}_f \left(\underbrace{\gamma_\mu \partial^\mu + \gamma_0 \cdot \mu + \sigma}_Q \right) \psi^f \right) \quad (3.4)$$

On the first view, the actions are very different, but the Hubbard-Stratonovich-Transformation shows, by integrating the quadratic scalar field σ out, that their path integrals are physically equivalent (summation over f is meant implicitly below):

$$\begin{aligned}
& \int D\sigma \exp \{-S[\bar{\psi}, \psi, \sigma]\} = \int D\sigma \exp \left\{ - \int d^2x \left(\frac{1}{2g^2} \sigma^2 + \bar{\psi}_f (\gamma_\mu \partial^\mu + \gamma_0 \cdot \mu + \sigma) \psi^f \right) \right\} \\
& = \exp \left\{ - \int d^2x \left(\bar{\psi}_f (\gamma_\mu \partial^\mu + \gamma_0 \cdot \mu) \psi^f \right) \right\} \cdot \int D\sigma \exp \left\{ - \int d^2x \left(\frac{1}{2g^2} \sigma^2 + \bar{\psi}_f \psi^f \sigma \right) \right\} \\
& = \exp \left\{ - \int d^2x \left(\bar{\psi}_f (\gamma_\mu \partial^\mu + \gamma_0 \cdot \mu) \psi^f \right) \right\} \cdot \left(\det \left[\frac{1}{g^2} \delta^{(2)}(x-y) \right] \right)^{-1/2} \\
& \times \exp \left\{ \frac{1}{2} \int d^2x g^2 \left(\bar{\psi}_f \psi^f \right)^2 \right\} \\
& = \left(\det \left[\frac{1}{g^2} \delta^{(2)}(x-y) \right] \right)^{-1/2} \exp(-S[\bar{\psi}, \psi]) \\
& = \mathcal{N} \exp(-S[\bar{\psi}, \psi])
\end{aligned} \tag{3.5}$$

Since σ is multiplied by $\bar{\psi}\psi$ in the new action, it takes the role of a mass which breaks chiral symmetry if it is unequal to zero. That is why the expectation value of the scalar field (called chiral condensate) expresses if chiral symmetry is restored or spontaneously broken, dependent on μ and T . σ 's expectation value can therefore, be used as the order parameter of the phase diagram. Its value is zero if homogeneous chiral symmetry is restored, non zero but constant in the phase with homogeneous chiral symmetry breaking and oscillating in the inhomogeneous phase called (chiral) crystal.

To finally get rid of the remaining dependence of ψ_f in the path integral, the following identity belonging determinant calculation via Grassmann valued fields can be used:

$$\int D\bar{\psi} D\psi e^{-\bar{\psi}_i Q \psi_i} = \prod_{i=1}^N \int D\bar{\psi}_i D\psi_i e^{-\bar{\psi}_i Q \psi_i} = \prod_{i=1}^N \det(Q) = \det(Q)^N \tag{3.6}$$

Additionally, N factorizes in the action and in the case of large- N , it is strongly repressed in the exponential. If N goes to infinity only the field configuration minimizing S_{eff} has necessary impact on a calculated expectation value just like in a classical limit.

$$\begin{aligned}
Z & = \mathcal{N} \int D\sigma \left(\det (\gamma_\mu \partial^\mu + \gamma_0 \cdot \mu + \sigma) \right)^N e^{-\int d^2x \frac{1}{2g^2} \sigma^2} \\
& = \mathcal{N} \int D\sigma \exp \left\{ -N \left(\int d^2x \frac{1}{2\lambda} \sigma^2 - \ln (\det (\gamma_\mu \partial^\mu + \gamma_0 \cdot \mu + \sigma)) \right) \right\} \\
& \Rightarrow S_{\text{eff}}[\sigma] := N \left\{ \int d^2x \frac{1}{2\lambda} \sigma^2 - \ln (\det (\gamma_\mu \partial^\mu + \gamma_0 \cdot \mu + \sigma)) \right\}
\end{aligned} \tag{3.7}$$

$\lambda = N \cdot g^2$ is the coupling constant of the effective action. Raising the determinant to the exponential by logarithm, requires it to be strictly positive, which will be shown later for the purely homogeneous case. A space dependent σ forces the determinant to be real [14], which ensures the transformation to be correct if the number of flavors is even.

Since the only contributing field configuration is the one minimizing the effective action $e^{-S_{\text{eff}}[\sigma]} \approx \text{const} \cdot \delta(\sigma - \sigma_{\text{min}})$, no path integral, but a minimization of S_{eff} in σ needs to be computed to calculate

expectation values.

$$\langle O \rangle = \frac{\int D\sigma O(\sigma) \cdot e^{-S_{\text{eff}}[\sigma]}}{Z} \approx \frac{O(\sigma_{S_{\text{min}}}) \cdot \text{const}}{\text{const}} = O(\sigma_{S_{\text{min}}}) \quad (3.8)$$

For generating a chiral phase diagram, the searched expectation value is the one of the field itself (the chiral condensate) i.e., only the minimum of S_{eff} needs to be computed in σ for various chemical potential and temperature.

The analytical solution of the GN model in 1+1 dimensions shows a phase diagram (see Figure 3.1) with a homogeneous broken phase for low temperature and chemical potential, a chirally restored phase for high temperature (and/or low chemical potential) and an inhomogeneous phase for low temperature and high chemical potential. The shape of the crystal is an oscillating function in space, whose wavelength shrinks for growing chemical potential.

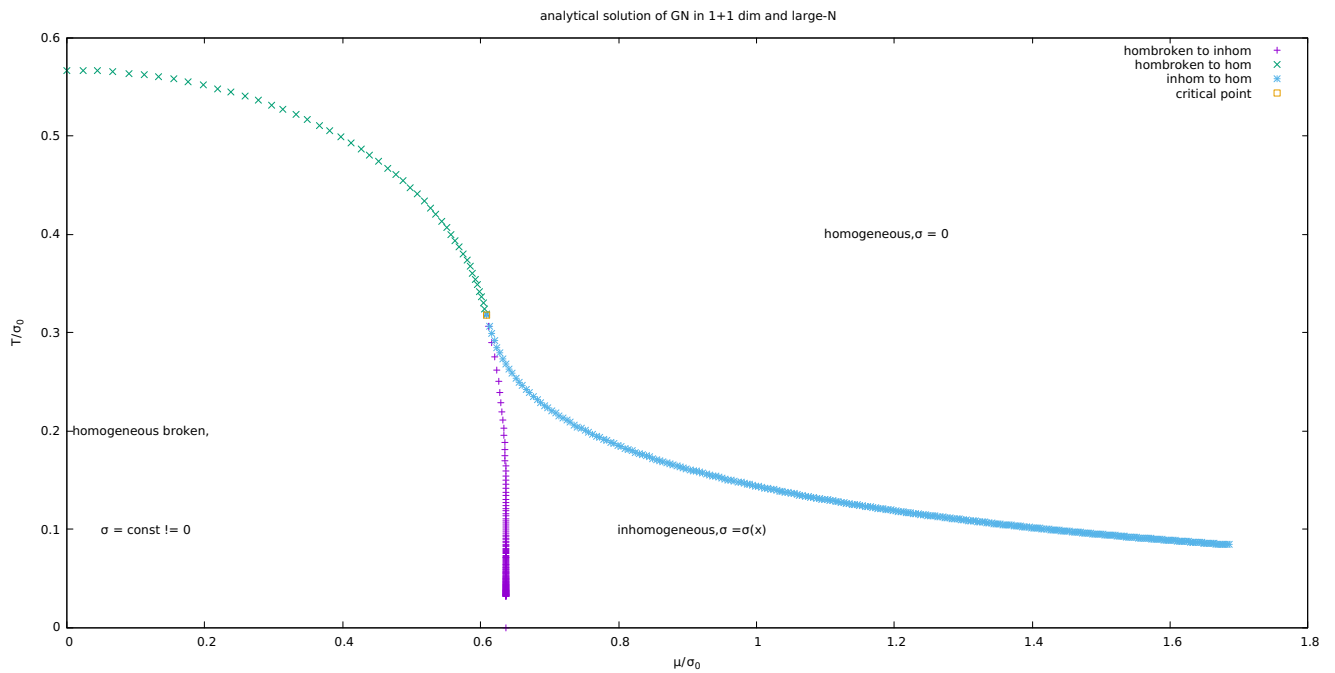


FIGURE 3.1: Analytical solution of the GN model in 1+1 dim and the large-N limit [3]

Chapter 4

Implementation

As explained in the introduction, the infinite dof's of a field theory need to be reduced from infinite to a finite number of variables. Developing the discretized effective action as a function of these variables is the aim of this chapter [6].

At first, the size of spacetime needs to be restricted. One chooses a space length L (in a higher dimensional case a volume V) and a time extension T_t (do not mix up with temperature T) with a kind of periodic boundary conditions. Two ways of reducing the still infinite dof's are presented in the following:

1. Lattice discretization: Similar to the described lattice QCD the spacetime becomes discrete by reducing it to a finite number of lattice points at which the field strength is one variable. The spacing between two lattice points is a in space and time direction. The number of lattice points in the respective direction is N_T and N_L .

$$\begin{aligned}(x, t) &\rightarrow (x_i, t_i) \\ \sigma(x) &\rightarrow \sigma(x_i) = \sigma_i\end{aligned}\tag{4.1}$$

$$\begin{aligned}x_i &\in [n \cdot a, \quad n = 0, \dots, N_L] \\ t_i &\in [n \cdot a, \quad n = 0, \dots, N_T]\end{aligned}\tag{4.2}$$

2. Expansion in a set of basis functions until a given cutoff: Any orthogonal basis functions can be chosen e.g. complex exponentials or trigonometrical functions (Fourier series). The higher the order i.e. the frequency, the lower is the effect on the resulting function. Therefore a cutoff is reasonable. The field variables are the amplitudes of the expansion.

$$\sigma(x) \rightarrow \sum_{n_x=1}^{N_L} a_{n_x} \cdot e^{in_x x}\tag{4.3}$$

Both opportunities have advantages and disadvantages [15]. The basis functions lead to a continuous $\sigma(x)$ as a solution but without a lattice, the determinant of the operator $Q = \gamma_\mu \partial^\mu + \gamma_0 \cdot \mu + \sigma$ also needs to be computed via continuous basis functions. That leads to a problem, because the result of Q acting on a basis function can leave the finite not complete function space and therefore spoil the computation. This is not occurring on a lattice, because the lattice basis functions are delta functions and Q acting on them produces in the worst case shifted delta functions on other spacetime points. But since the lattice has (anti)periodic boundary conditions, the space of functions can not be left. The disadvantage of lattice discretization is the fermion doubling effect which means, that the number of flavors is doubled.

Here, a combination of both, using the advantages and avoiding the disadvantages is performed: Lattice discretization in space direction with periodic boundary conditions ($f(x) = f(x + L)$) and $\sin(\omega_i \cdot t)$, $\cos(\omega_i \cdot t)$ basis function expansion with antiperiodic boundary conditions ($g(t) = -g(t + T_i)$) in time direction. The basis functions in time are eigenfunctions (actually complex exponentials are the eigenfunctions, but this is equivalent to a 2 dimensional \sin, \cos vector and a complex number implementation is avoided) of the time dependent part of Q . Therefore the matrix Q is diagonal in time direction. Q acting on its eigenfunctions does not change them (except a factor) and therefore the finite function space is never left. To not take infinitely many eigenfunctions in account is reasonable because Q acting on higher order time eigenfunctions produces additional terms proportional to the growing frequency ω_i . Therefore higher order eigenvalues λ_i get less dependent on σ :

$$\ln(\det(Q)) = \ln\left(\prod_i \lambda_i\right) = \sum_i \ln(\lambda_i) \propto \sum_i \ln(\omega_i) \quad (4.4)$$

It follows, that high order eigenfunctions do only add constants to the action, but constant values do not change the dynamics of a system and can be neglected. The fermion doubling on the lattice is not a problem, because GN is in the large-N limit and a doubling of infinity is irrelevant.

Field discretization:

$$\sigma(x) \rightarrow \sigma(x_i) = \sigma_i \quad (4.5)$$

(Hereinafter x is meant to be the spatial index)

Orthogonal basis functions for calculating the determinant:

$$\begin{aligned} |f_m\rangle &= \frac{g(\omega_n t)}{\sqrt{2 \cdot L}} \cdot \delta_{B,A} \cdot \delta_{y,x} \quad m = (g, n, A, x), \quad g \in (\sin, \cos) \\ \omega_n &= \frac{2n - 1}{T_t} \cdot \pi \end{aligned} \quad (4.6)$$

Where A is the Dirac matrix index and ω_n follows from the antiperiodic boundary conditions in time direction.

Since the absolute time and space length has no meaning to the computer, the density of lattice points in L or modes in T can be chosen. A natural choice, that implies equal dof density in space and time is:

$$\begin{aligned} \frac{L}{N_L} &= a =: 1 \rightarrow \text{Cutoff} : x = a \\ \frac{T_t}{N_T} &= \frac{2\pi}{\omega_{\text{cut}}} =: 2 \rightarrow \text{Cutoff} : \omega_{\text{cut}} = \pi \end{aligned} \quad (4.7)$$

(ω_{cut} is between the last mode inside and the first mode outside)

For the calculation of the determinant, the operator Q is brought into matrix form by using the basis functions $|f_m\rangle$:

$$\begin{aligned} \langle f_m | Q | f_{m'} \rangle &= (\gamma_0)_{A,A'} \cdot \left\langle \frac{g(\omega_n t)}{\text{sqrt}(2L)}, \omega_{n'} \cdot \frac{\partial g'(\omega_{n'} t)}{\text{sqrt}(2L)} \right\rangle \cdot \delta_{x,x'} + \mu \cdot \left\langle \frac{g(\omega_n t)}{\text{sqrt}(2L)}, \frac{g'(\omega_{n'} t)}{\text{sqrt}(2L)} \right\rangle \cdot \delta_{x,x'} \\ &+ (\gamma_1)_{A,A'} \cdot \left\langle \frac{g(\omega_n t)}{\text{sqrt}(2L)}, \frac{g'(\omega_{n'} t)}{\text{sqrt}(2L)} \right\rangle \cdot \frac{\delta_{x,x'-a} - \delta_{x,x'+a}}{2a} \\ &+ \delta_{A,A'} \delta_{x,x'} \sigma(x') \left\langle \frac{g(\omega_n t)}{\text{sqrt}(2L)}, \frac{g'(\omega_{n'} t)}{\text{sqrt}(2L)} \right\rangle \end{aligned} \quad (4.8)$$

$$\text{with } \partial_x \rightarrow \partial_{x,x'} = \frac{\delta_{x+a,x'} - \delta_{x-a,x'}}{2a}$$

$$\text{and } \langle g, g' \rangle = \delta_{n,n'} \cdot \begin{pmatrix} 1 & 0 \\ 0 & 1 \end{pmatrix} \quad \langle g, \partial g' \rangle = \delta_{n,n'} \cdot \begin{pmatrix} 0 & 1 \\ -1 & 0 \end{pmatrix}$$

An useful information from this derivation is, that the matrix Q is translational invariant in x as long as all σ_i 's have the same value.

If σ is purely homogeneous, the determinant is easy to compute, since the spatial eigenvectors of the discretized lattice derivative are obvious just complex exponentials with the wavenumber $k = \frac{2\pi n}{L}$ for the n 'th eigenvector (from the periodic boundary conditions) and e^{ikx} corresponding to the x 'th latticepoint as entries. The eigenvalues to the n 'th eigenvector are $\sin(\frac{2\pi na}{L})$ [6]. So one just needs to calculate all eigenvalues of Q and multiply them to compute the determinant. Only in Dirac space the determinant needs to be calculated explicitly, which is simple, since it is just a 2x2 matrix.

$$\begin{aligned} \det(Q) &= \prod_{n=-N_T+1}^{N_T} \prod_{x=0}^{L-1} \det(\gamma_0 \cdot (\frac{i \cdot (2n-1)\omega_{cut}}{2N_T} + \mu) + \gamma_1 \cdot i \cdot \sin(\frac{2\pi x}{L}) + \sigma) \\ &= \prod_{n=1}^{N_T} \prod_{x=0}^{L-1} (A(\sigma^2)^2 + B^2) > 0 \end{aligned} \quad (4.9)$$

with $\gamma_0 = \begin{pmatrix} 0 & 1 \\ 1 & 0 \end{pmatrix}$ and $\gamma_1 = \begin{pmatrix} 1 & 0 \\ 0 & -1 \end{pmatrix}$ the first, third Pauli-matrix and A, B are functions whose explicit form is not of interest in the following.

The determinant is positive definite and therefore the prior rising by logarithm to the effective action was correct. The analytical expression allows further simplifications due to the later out needed derivatives of the action.

If space dependence of the field is permitted ($\sigma \doteq \sigma_i$), the calculation of the determinant is difficult, because no spatial eigenvectors are obvious. Therefore the determinant is calculated explicitly by the linear algebra library GSL.

The discretized effective action is:

$$\begin{aligned} S_{\text{eff}} &= \frac{1}{2\lambda} \cdot \left(\int_0^L dx \int_0^{T_t} dt \sigma(x)^2 - \ln(\det(Q(\sigma(x)))) \right) \\ &\rightarrow \frac{1}{2\lambda} \cdot 2N_T \cdot a \cdot \sum_{x=1}^L \sigma_x^2 - \ln(\det(\langle f_m | Q(\sigma(x)) | f_{m'} \rangle)) \end{aligned} \quad (4.10)$$

The computation starts with the calculation of the coupling constant λ , by inserting a critical time extension $N_{T,c}$ (it needs to be at least 10 to 15 times smaller than L , to get pictures close to the analytical solution), a space extension L and $\mu = 0$. The coupling constant is chosen to a value, so that the second order transition (sign change of second derivative in $\sigma = 0$) from homogeneous broken to homogeneous matches with $N_{T,c}$. After that, the value of σ at $T = 0$, $\mu = 0$ called σ_0 ($T = 0$ corresponds to a very great time extension $N_{T,0}$) is computed. In the phase diagram, the values T, μ and σ get physical meaning by dividing them by σ_0 , since in physics comparisons between variables of the same problem and in the same unit count. The natural unit system gives them the same physical unit, since they are added in the determinant calculation. With correct proportions, the diagram is completely physical and one can compare the analytical phase boundaries to the numerical ones.

Chapter 5

Homogeneous phase diagram

In the following chapter, the phase diagram of a purely homogeneous sigma (space independent) will be computed and analyzed. The homogeneous phase diagram was thought to be the correct solution of the GN model, until the 2000's, when an inhomogeneous $\sigma(x)$ led in some phase diagram regions to a deeper minimum than before [3]. But the homogeneous diagram is still interesting, since the phase boundary from homogeneous broken to homogeneous is the same as in the space dependent case and can be calculated in way less computation time, since it is an one dimensional problem. Additionally, the methods for the inhomogeneous calculation can easier be developed in one dimension and later be generalized to the multidimensional function.

Two ways of finding phase boundaries are used: Minimization by a GSL function and stability analysis in $\sigma = 0$. A necessary condition for the stability check is an extremum in zero in all phases, since it detects for which μ at a given temperature T the minimum in the homogeneous phase changes to a maximum in the homogeneous broken phase. Therefore, the minimum needs to be shifted continuously out of zero at the phase boundary so that a maximum remains. This is called a second order phase transition. The second derivative (the curvature) changes its sign when the minimum in zero changes into a maximum and that is why its root can indicate a phase boundary. Additionally the action needs to be symmetric with respect to zero because a non symmetric one could enable saddles instead of maxima and minima, which would spoil the computation.

Proof symmetry of $S(\sigma)$:

$$S_{\text{eff}}(-\sigma) = \text{const} \cdot (-\sigma)^2 - \sum_{n_i} \sum_x \ln(A((-\sigma)^2)^2 + B^2) = S_{\text{eff}}(\sigma) \quad (5.1)$$

The proof actually also shows that the action has an extremum in $\sigma = 0$. The analytically known homogeneous phase diagram has a second order phase boundary coming from high temperature and low chemical potential until a critical point, where it changes to a first order transition moving to low temperature and higher chemical potential. The second order phase boundary can successfully be found by stability analysis, what can be looked up in Figure 5.2 where a maximum in zero appears in contrast to figure 5.1. This procedure is not working for the first order transition, because in this case a local minimum remains in zero and new deeper valleys appear in a not vanishing distance to zero (see figure 5.3), which spoils the computation. The local minimum disappears deeper in the homogeneous phase (lower chemical potential) and therefore a pseudo 2nd order phase boundary can be calculated (see Figure 5.4). The first order transition can only be detected by a minimization of the effective action i.e., the phase points have to be found, where the minima in zero and out of zero have equal depth. First order transitions can also occur in other models and therefore the stability analysis results are not valid but can give a first and fast impression, how a phase boundary maybe looks like. The values for temperature and chemical potential, the action is plotted at, can be referred to the phase diagram in figure 3.1.

Finally, a phase diagram for the homogeneous σ case can be plotted and since σ is a number, a 3d plot can be generated by minimizing the action for various chemical potential and temperature (see Figure 5.5). As visible, the first order transition is related to a jump in the phase diagram, because the value of the chiral condensate changes discontinuously. The second order transition corresponds to a kink in the order parameter, since the order parameter moves continuously out of zero.

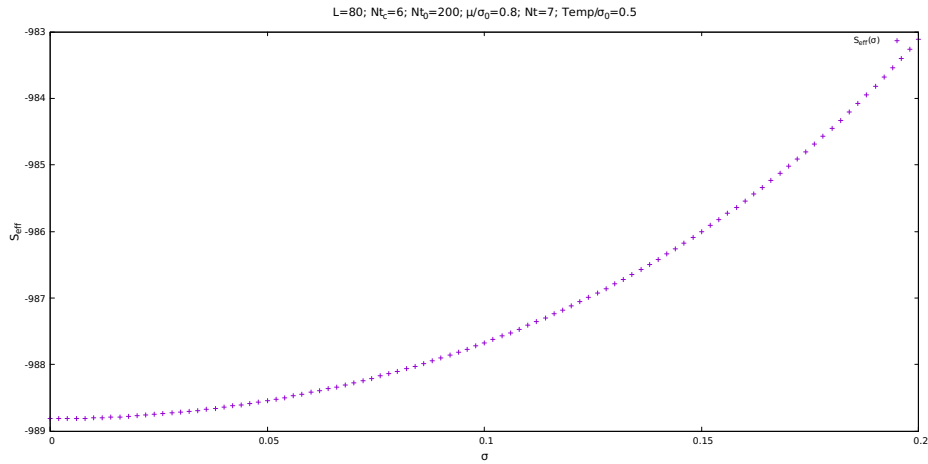


FIGURE 5.1: Homogeneous phase

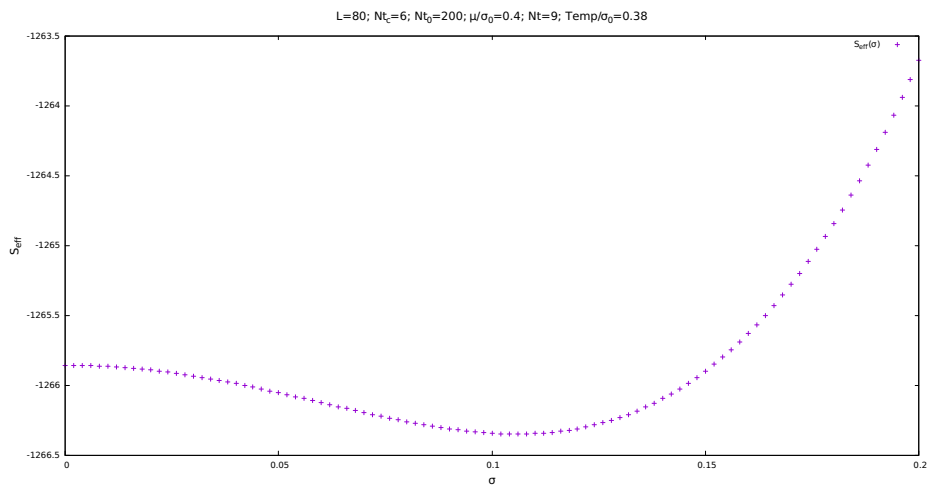


FIGURE 5.2: Homogeneous broken phase and second order transition region

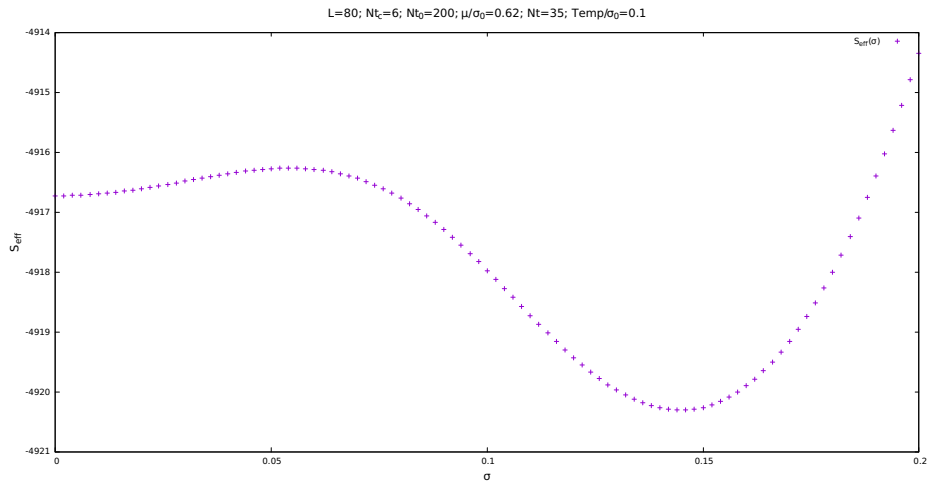


FIGURE 5.3: First order transition region

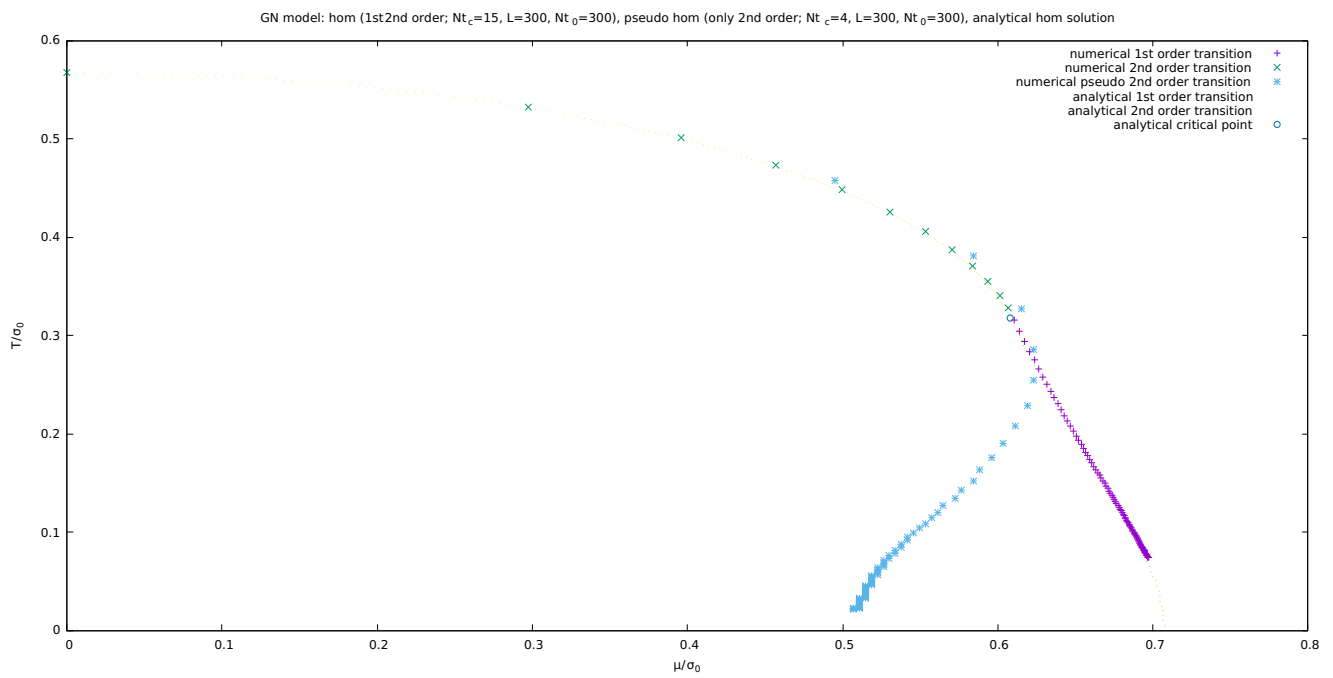


FIGURE 5.4: Pseudo second order transition in first order transition region

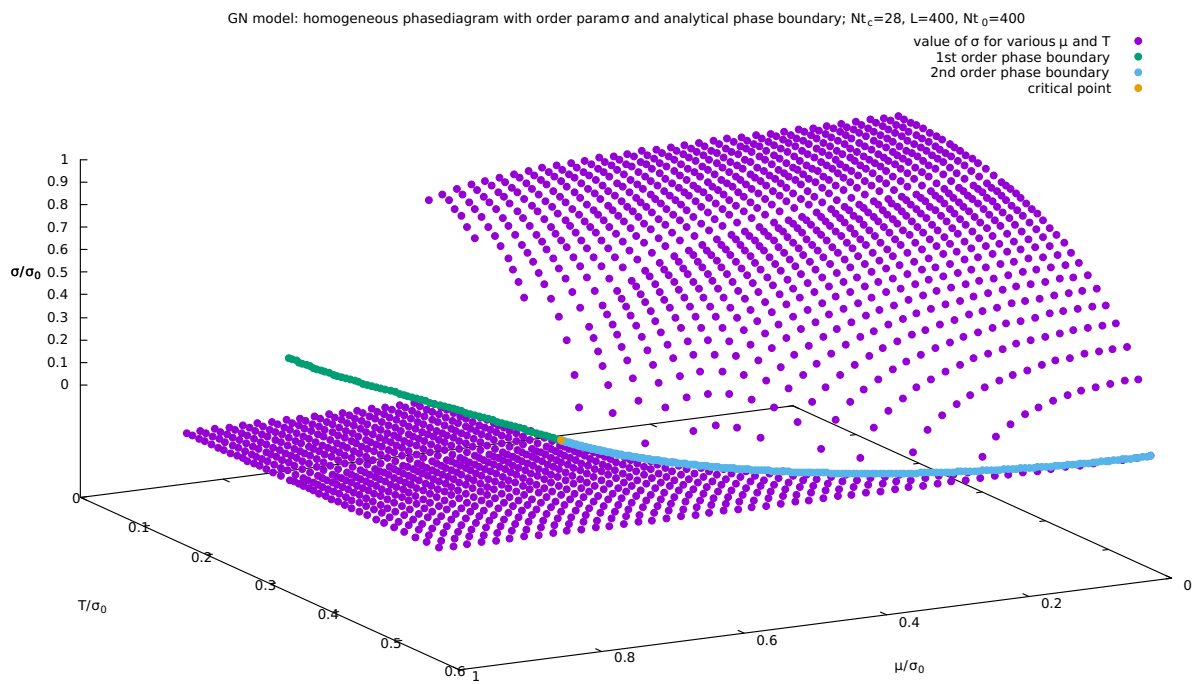


FIGURE 5.5: 3d phase diagram of the homogeneous GN model in 1+1 dim

Chapter 6

Inhomogeneous phase diagram

If σ is allowed to be space dependent, the solutions change in comparison to the homogeneous case and an inhomogeneous region in the phase diagram occurs for high chemical potential and low temperature (see Figure 3.1). The critical question is, if this behavior also appears in QCD and therefore simple and time saving numerical algorithms are needed to perform them on other QCD inspired models. The effective action is now a function in many variables σ_i . The minimum can, as in the purely homogeneous case, be found in different ways. The here chosen option is stability analysis for 2nd order phase boundaries at $\sigma_i = 0$ (i.e. only transitions to the homogeneous phase can be detected). Since zero becomes a global minimum for all σ_i in the homogeneous phase and hopefully somehow unstable, but still an extremum, in other phases. There is, like in the purely homogeneous case no guarantee for instability in zero at a transition from the homogeneous to nonhomogeneous phases, since a local minimum could remain in zero (1st order transition). This is not the case in the inhomogeneous GN model; all phase transitions are of 2nd order [3]. Therefore, the predictions for other models by this methods should be treated with caution and should only give an idea of the phase diagram.

In analogy to the homogeneous case the symmetry of the effective action implying the existence of a local extremum in all phases in $\sigma_i = 0$ is a necessary condition to perform a stability analysis. Both is not proven analytically yet, but numerical tests imply, that it holds. The Hessian matrix is the needed object to investigate in hyperdimensional stability analysis.

$$(H_{S_{\text{eff}}}(\vec{\sigma}))_{ij} = \left(\frac{\partial^2 S_{\text{eff}}(\vec{\sigma})}{\partial \sigma_i \partial \sigma_j} \right)_{ij} \quad (6.1)$$

Diagonalizing this matrix yields eigenvalues that describe the local curvature (like the second derivative in the one dimensional case) in the direction of the corresponding eigenvector, e.g. in $\sigma_i = 0$.

$$\forall \lambda_i \begin{cases} > 0, & \text{Minimum in the eigenvector direction} \\ < 0, & \text{Maximum in the eigenvector direction} \end{cases} \quad (6.2)$$

If both, positive and negative eigenvalues appear, the function has an unstable extremum in zero called a saddle. A positive lowest eigenvalue indicates, that all directions have positive curvature i.e. the action is parabolic and the homogeneous phase is occurred. Comparable to the homogeneous case the root of the lowest eigenvalue function indicates the transition.

The numerical calculation of the Hessian matrix in $\vec{\sigma} = 0$ proceeds by building the differential quotient for a finite but sufficiently small ϵ twice. The resulting formulae for nondiagonal elements is:

$$(H_{S_{\text{eff}}})_{ij} = \frac{S_{\text{eff}}(\sigma_i = \sigma_j = \epsilon) - S_{\text{eff}}(\sigma_i = -\epsilon, \sigma_j = \epsilon) - S_{\text{eff}}(\sigma_i = \epsilon, \sigma_j = -\epsilon) + S_{\text{eff}}(\sigma_i = \sigma_j = -\epsilon)}{4\epsilon^2} \quad (6.3)$$

While for the diagonal elements it reads:

$$(H_{S_{\text{eff}}})_{ii} = \frac{S_{\text{eff}}(\sigma_i = \epsilon) - 2 \cdot S_{\text{eff}}(\sigma_i = 0) + S_{\text{eff}}(\sigma_i = -\epsilon)}{\epsilon^2} \quad (6.4)$$

All other σ_k entries are zero.

The calculation of the matrix can be accelerated by using symmetries of the Hessian matrix.

1. It is real and symmetric: $H_{ij} = H_{ji}$. Only the upper or lower triangular part of the matrix needs to be calculated.

2. As shown in the implementation, the matrix Q and therefore also the effective action are translational invariant, if all σ_i entries are equal (the quadratic field term has an even higher degree of symmetry since all σ_i are equally treated). This means that the entries of H_{ij} only depend on differences between their indices (or on the magnitude of the difference, when using the symmetry). Therefore every row can be copied to the next by a shift of one. Additionally, the space is periodic i.e. a circle and the indices L and zero are equal. Because of that, index differences over L also count, i.e. only the first half row needs to be calculated.

$$H = \begin{pmatrix} H_{00} & \dots & H_{1\frac{L}{2}} & \dots & H_{00} \\ H_{01} & \ddots & & & \\ \vdots & & & & \end{pmatrix} \quad (6.5)$$

A bisection of the lowest eigenvalue function can be performed for a given temperature and the root marks the corresponding chemical potential at a second order phase transition. The eigenvector belonging to the lowest eigenvalue indicates the direction of steepest descent in zero. It does not necessarily need to point to the global minimum, since local minima near of zero can arise, except at the phase boundary to the homogeneous phase. There the global minimum needs to move continuously out of zero (2nd order transition) and is therefore, the nearest one.

The phase boundaries from homogeneous broken to homogeneous and from inhomogeneous to homogeneous are in good accordance with the analytical results. The crossing from homogeneous broken to inhomogeneous cannot be detected in this way, because σ is not zero at the transition. Nevertheless, the results of the inhomogeneous to homogeneous transition do not match with the analytical solution as good as the crossing from homogeneous broken to homogeneous. The reason is a finite volume effect [1], that distort the results. Since the phase boundary points were calculated by a bisection of the lowest eigenvalue function, it is meaningful to plot this function to search for systematical mistakes [2] (see Figure 6.1, violet dots). The resulting function is continuous but not smooth. The reason is, that the finite volume box with periodic boundary conditions does not enable arbitrary wavelength of the chiral condensate. If the wavelength minimizing the effective action is not an integer divider of the box length L , it is not adopt because the periodic boundary conditions forbid it, but the next closest wavelength, which is a divider. The new (allowed) minimum of the action lies not as deep as the original one and therefore the curvature in zero is increased. This behavior reaches a maximum at a wavelength that would fit $n + \frac{1}{2}$ times into the box, since this is the length most far away from matching. Consequently the lowest eigenvalue function shows unphysical peaks/heels and therefore, its root is falsified. For a growing number of lattice points, this effect lowers e.g. for a doubling of lattice points, a former peak is split into two smaller ones [1]. In the infinite volume limit $L \rightarrow \infty$, the process should therefore vanish [1]. The effect does not occur at the phase transition from homogeneous to homogeneous broken, since the minimum that arises and moves out of zero, is in this case not an oscillating, but spatially constant

σ and therefore no wavelength need to fit into the box.

Getting a more realistic root for the lowest eigenvalue, that is closer to the continuum solution is the goal of the algorithm described below. Principally the valleys of the lowest eigenvalue function are continuum solutions and fitting a function on them lead to a good approximation of the thermodynamic limit solution in a close area. Since polynomial functions of order lower 3 are easy to handle, a parabolic fit, as well as a linear one, are used:

- calculate the root μ_{prev} of the lowest eigenvalue graph by bisection
- improve for $\frac{\mu_{prev}}{\sigma_0} > 0.6$ (inhom to hom transition), store pairs of (μ, λ_{min}) in an 1d array, choose a stepsize $\approx 0.02 \cdot \sigma_0$ (used in this thesis)
- search to the left (by Peakseeker method) until two peaks are found (add elements in front of the array by push back)
 - less than 2 peaks after 40 calculations, return previous root
- search to the right (by Peakseeker method) until two peaks are found (add elements in the back)
 - less than 2 peaks after 40 calculations, return previous root
- first valley estimate: middles between peaks, these points named plotpoints
 - generate a parabola through these 3 points e.g. calculate the parabola for all μ values than the original smallest eigenvalue function
- compare the parabola and lowest eigenvalue points
 - replace the closest plotpoint if a lowest eigenvalue lies deeper
 - * generate a parabola through these 3 points e.g. calculate the parabola for the μ values the original function is calculated for
 - if one or many replacements took place start again with the comparison, stop that process after 10 iterations
- return the root of the parabola (check whether the left or right root by examining the sign of the purely quadratic term)
 - if the root is complex (i.e. none of the valleys is higher than zero), expand the lowest eigenvalue function to the right until a new peak is found
 - remove the most left plotpoint and add one to the right
 - * generate a parabola through these 3 points
 - start again with the comparison
 - repeat this expansion process maximal 3 times
 - * no real result, return previous root

Peakseeker method:

- The slope (since the stepsize is constant, focus on functional differences) grows until an edge and shrinks abruptly after it; therefore: $f_0 - f_1 < f_1 - f_2$ indicates an edge. (Problem: This inequality corresponds to negative curvature i.e. a hill)

- If the peak is a maximum, the edge seeker would indicate peaks everywhere between the two belonging turning points, because the curvature is negative there. To prohibit that, the algorithm blocks new peak observation if one edge was found until the edge algorithm returns no more peaks at one go. (Note: If a maximum appears, the peak is not detected precisely, but this does not matter, because only a rough approximation is needed since the parabolic improvement changes the plotpoints anyhow)

The parabola can be calculated via three plotpoints by using its general form:

$$f(x) = ax^2 + bx + c$$

inserting the points and rearrange for a, b and c.

The algorithm of linear root approximation is similar, except that two instead of one plotpoints and the general form of a linear function are used.

The resulting plot for 80 lattice points, 8 as the critical number of time basis functions and a temperature of 70 looks as follows:

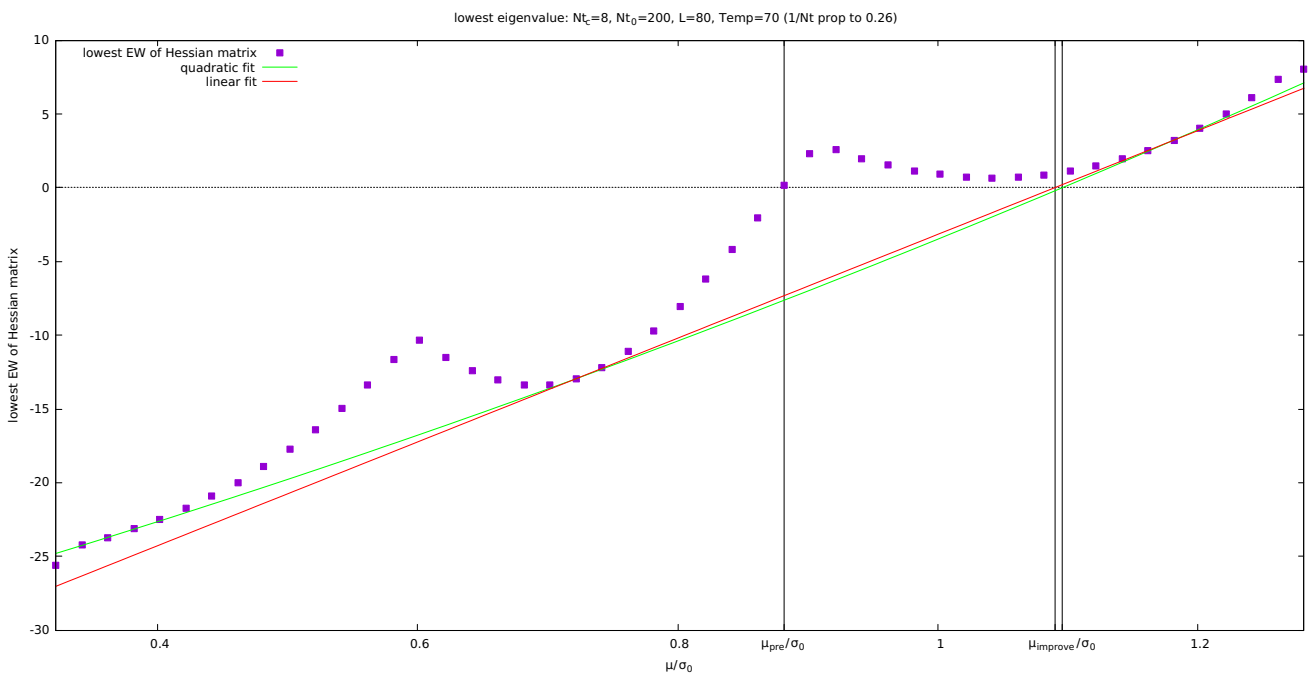


FIGURE 6.1: Lowest eigenvalue function and valley fit improvement

The parabolic (green) and linear (red) fits on the valleys of the lowest eigenvalue function (violet) (see Figure 6.1) do not differ much, but for growing μ the linear approximation yields worse results than the parabolic one. In the phase diagram the parabolic improved results (green) are shown in comparison to the unimproved bisection results (violet) and the analytical ones (black dotted). For growing μ the improved results get worse (see Figure 6.2).

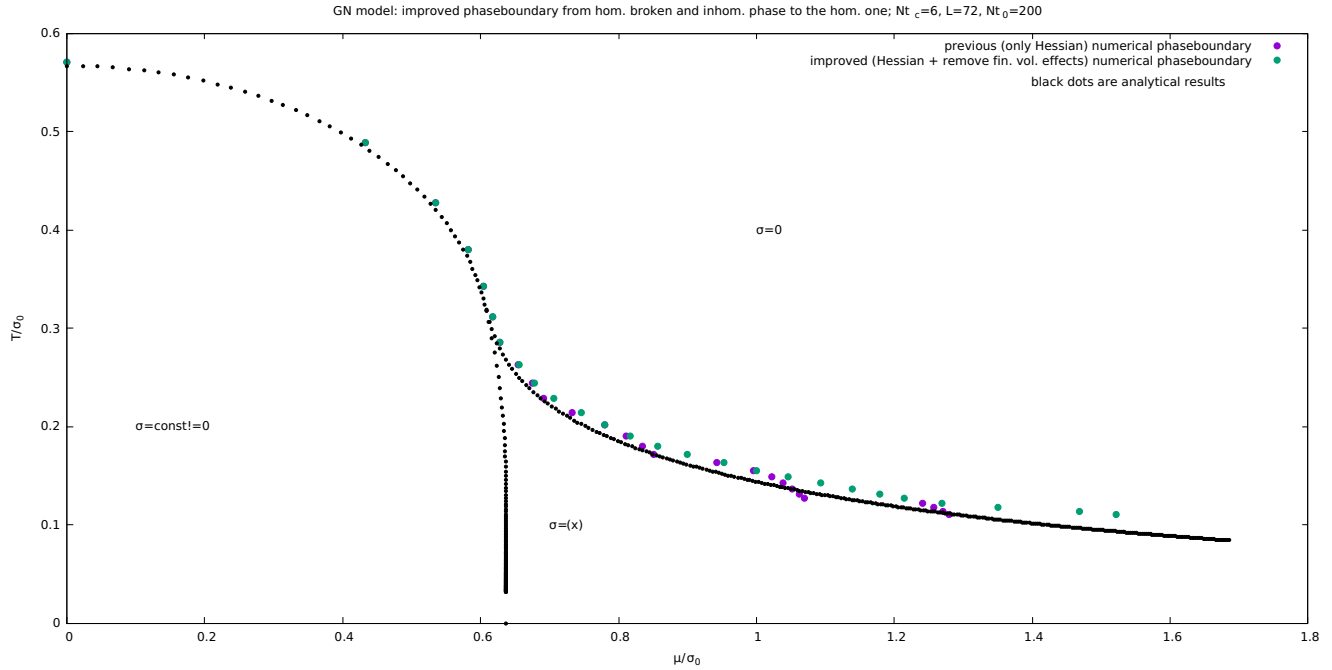


FIGURE 6.2: 2d phase diagram of the space dependent GN in comparison to the analytical results

As explained before, it is possible, that the eigenvector corresponding to the lowest eigenvalue points to the global minimum, if no other spoiling local minima are closer to zero (especially close to homogeneous phase boundaries, there is a good chance, because the global minimum arises from zero). In that case, the entries of the eigenvector are a good approximation for the spatial shape of the chiral condensate. Numerical tests show, that the eigenvector entries behavior in the inhomogeneous phase matches to the analytical oscillating function, and can therefore be used as a first approximation of the chiral condensate, which needs to be substantiated by a real minimization. It looks as follows for various μ and fixed temperature. The wavelength of the crystal shrinks as expected for growing chemical potential (see Figure 6.3 & 6.4).

But that the eigenvectors point to the global minimum is not necessarily the case. Numerical tests in the homogeneous broken phase, show an eigenvector that points to a local minimum, which shows a nonconstant shape for the chiral condensate. That is why the phase border from the inhomogeneous to homogeneous broken phase cannot be detected via the distinction of constant or nonconstant eigenvector entries. The reason, that local minima are closer to zero is, that the phase transition from inhomogeneous to homogeneous broken happens in a nonvanishing distance to zero. The global minimum of the inhomogeneous phase comes closer to a homogeneous broken solution i.e., the wavelength of the crystal grows until it is infinity (as long as the box), but the amplitude (distance to zero) is never zero.

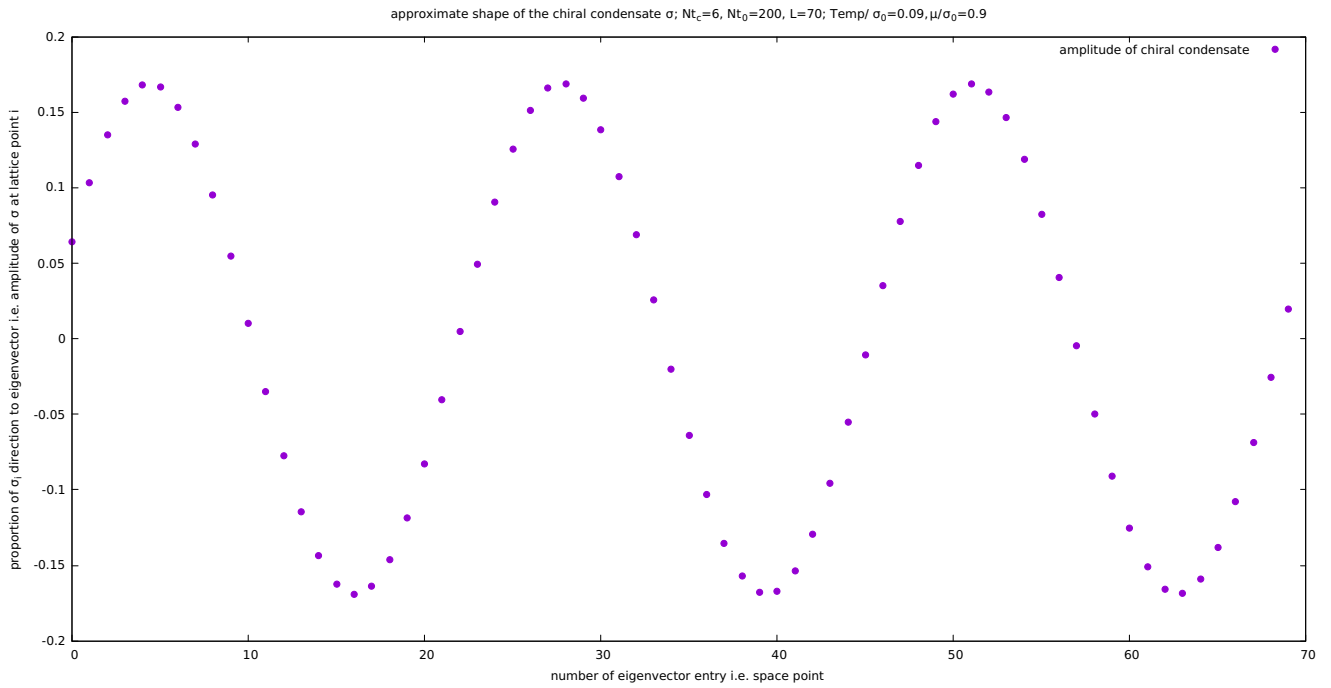


FIGURE 6.3: Shape for low chemical potential

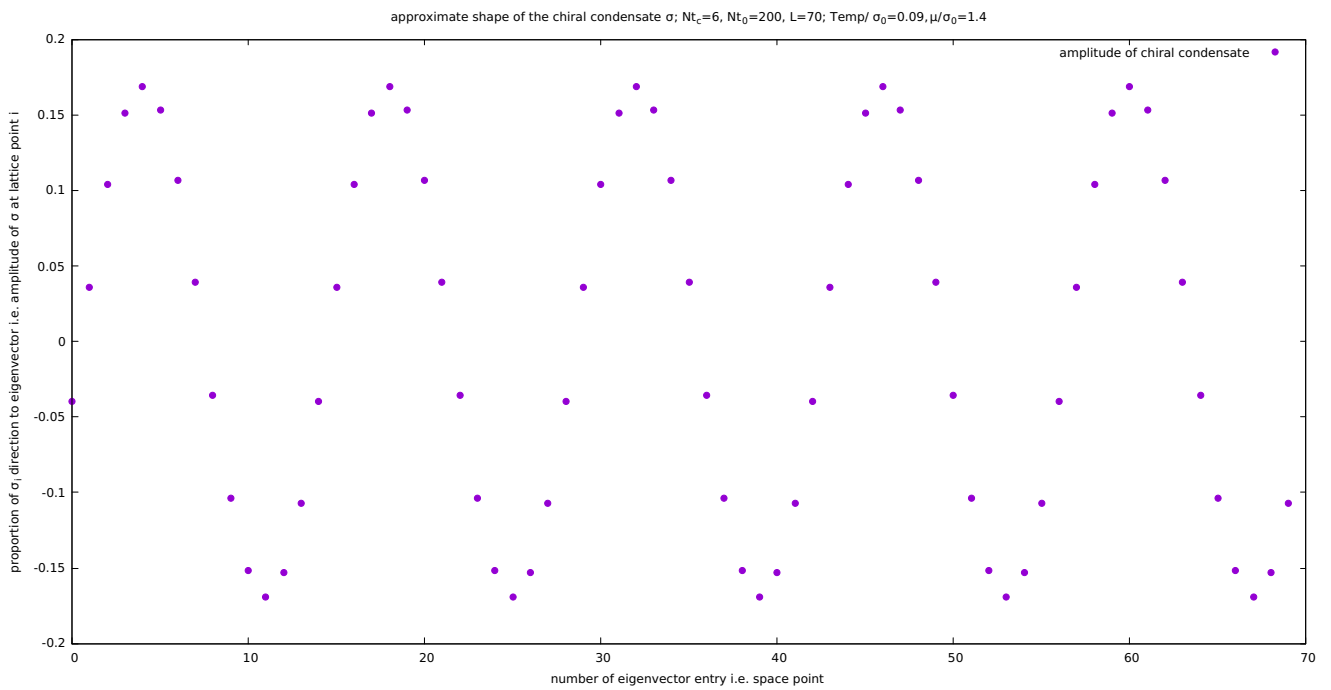


FIGURE 6.4: Shape for high chemical potential

Chapter 7

Computing time improvements

The calculation of all eigenvalues of the Hessian matrix is relatively time consuming, although only the smallest one is of interest. Calculating the improved phase diagram takes for an acceptable but small box length $L \approx 60$ at least half a day (Lenovo ThinkPad L420 i5). The situation will become even worse if a model in higher dimensions is going to be investigated prospectively, because the number of variables grows by a factor of L for every dimension. Therefore 4 methods are investigated which were candidates to speed up the eigenvalue calculation. The first two subsections and their algorithms are partially new developments of this thesis.

7.1 Determinants of first minors

First minors are square submatrices of the original matrix A , starting from the left upper end. Determinants of them are represented by Δ_i [23]:

$$A = \begin{pmatrix} a_{11} & a_{12} & \dots \\ a_{21} & \ddots & \\ \vdots & & \end{pmatrix} \quad (7.1)$$

$$\Delta_1 = a_{11}, \quad \Delta_2 = \det \begin{pmatrix} a_{11} & a_{12} \\ a_{21} & a_{22} \end{pmatrix}, \quad \dots$$

The interesting property of the first minors is, that all of them are positive definite, if the original matrix is it too [23]. Positive definiteness of a matrix means, that all its eigenvalues λ_i are bigger than zero:

$$A \text{ positive definite} \Leftrightarrow \Delta_i > 0 \Leftrightarrow \lambda_i > 0 \quad (7.2)$$

Therefore a determinant of a first minor smaller than zero indicates, that eigenvalues lower than zero exist i.e. the phase point does not lie in the homogeneous phase. The method could only be used if the value of the smallest eigenvalue is not needed explicitly (but the information if an eigenvalue smaller than zero exists), which is only the case for the bisection to find the first assumption of the lowest eigenvalue root. In a positive scenario, the entry a_{11} is always negative if a nonhomogeneous phase is adopt. In a negative scenario e.g. in the homogeneous phase, all first minor determinants need to be calculated to realize, that no eigenvalue is smaller than zero. The question is, if calculating some small determinants, but also a lot of big ones is more effective then calculating only big ones.

The calculation of determinants happens most effective and sturdily via LU decomposition (in German: LR Zerlegung) e.g. by the function `gsl_linalg_LU_det` in GSL. A matrix A is decomposed into a normalized lower triangular matrix L with ones on the diagonal and an upper triangular matrix U

with the eigenvalues on the diagonal from which the determinant can be calculated (since L has only ones on the diagonal its determinant is also one and following the determinants of U and A need to be the same) [13]. The LU decomposition works similar to the Gaussian Jordan algorithm since from the defining equation for each row of the $n \times n$ matrix A , n solvable equations appear, if the former row is calculated.

$$\begin{aligned} A_{jk} &= \sum_{i=1}^n L_{ji} \cdot U_{ik} \\ A_{0k} &= L_{00} \cdot U_{0k} = U_{0k} \\ A_{1k} &= L_{10} \cdot U_{0k} + L_{11} \cdot U_{1k} = L_{10} \cdot A_{0k} + U_{1k} \\ A_{2k} &= \dots \end{aligned} \quad (7.3)$$

For every square matrix, a LU like decomposition exists. Nevertheless, the condition for a LU decomposition: ($\det(\Delta_i^A) \neq 0$), is not necessarily fulfilled. This inconsistency is removed by introducing row exchanges in form of a pivoting matrix P acting on A [24]. P only changes the determinant by a factor of -1. The complexity of LU decomposition is of order $O(n^3)$ [7].

With that information the complexity of the first minor algorithm in the homogeneous phase can be calculated. The size of the first minors grows from one until the order of A :

$$\sum_{i=1}^n O(i^3) = O\left(\frac{n^2}{4} \cdot (n+1)^2\right) = O(n^4) \quad (7.4)$$

The complexity in the homogeneous phase is of order $O(n^4)$ and therefore the computing time in the phases with chiral symmetry breaking is irrelevant, because other algorithms of order $O(n^3)$ that calculate all eigenvalues are common. That is why the algorithm using first minors is not practical and saves no time.

7.2 Shifted matrix combined with power method

The power method is an iterative algorithm to find the eigenvalue with the biggest magnitude of an arbitrary matrix A [20] Its algorithm is:

Choose an arbitrary initial vector $y = y_0$

- $v = \frac{y}{|y|}$
- $y = Av$
- $\theta = v^T y$
- if $y - \theta v < \epsilon$, return θ as eigenvalue with biggest magnitude.

Proof of convergence (k=Iteration and power):

The initial vector y_0 is a linear combination of all eigenvectors v (since the eigenvectors of a full rank square matrix span a basis of the corresponding space): $y_0 = \sum_{i=1}^n \alpha_i \cdot v_i$

$$y_k = A^k \cdot y_0 = \sum_{i=1}^n \alpha_i \cdot \lambda_i^k \cdot v_i = \lambda_{max}^k \sum_{i=1}^n \alpha_i \cdot \left(\frac{\lambda_i}{\lambda_{max}}\right)^k \cdot v_i \rightarrow \alpha_{\lambda_{max}} \cdot \lambda_{max}^k \cdot v_{\lambda_{max}} \quad (7.5)$$

Where only the fraction with λ_{max} in the nominator does not vanish for great k . No sign is computed since the stretched eigenvector is projected on itself and therefore the scalar product is always positive. The problem about the method is, that the convergence is obviously dependent on the difference

between the two eigenvalues with the biggest and the second biggest magnitude. Therefore no exact complexity can be declared but the occurring matrix vector multiplication is at least of order $O(n^2)$. If the spectrum of eigenvalues is approximately known, one can choose an upper estimate shift matrix, to make all eigenvalues negative:

$$\begin{aligned}
 A \cdot v &= \lambda v \quad | \cdot c \cdot \mathbf{1} \cdot v \\
 (A + c \cdot \mathbf{1})v &= (\lambda + c)v \\
 \Rightarrow S &= (A + c \cdot \mathbf{1}) \\
 \Rightarrow \lambda' &= \lambda + c \\
 \lambda'_{max} &< 0
 \end{aligned} \tag{7.6}$$

Where the identity multiplied by the shift c is the shift matrix.

Letting the power method act on S one receives the former lowest eigenvalue which has the biggest magnitude after the shift:

$$|\lambda'_{min}| \Rightarrow \lambda_{min} = c - |\lambda'_{min}| \tag{7.7}$$

The reason not to choose an arbitrary large shift is, that the fraction of the two biggest eigenvalues will come closer to one and therefore the convergence is slower. That is why the shift should be chosen as small as possible to make all eigenvalues smaller than zero.

In case of the lowest eigenvalue function, the spectrum can be computed several times by a program that computes all eigenvalues to find an upper bound and after that, the shifted power method can be used. If it saves time, needs to be tested experimentally (see chapter 7.4).

7.3 Eigenvalue calculation via Tridiagonalization and QR decomposition (GSL and LAPACK)

The freeware libraries GSL (in C++) and LAPACK (in Fortran) are taken into account for the calculation of eigenvalues for symmetric $n \times n$ matrices. The function in GSL is: `gsl_eigen_symm_v`, that calculates the eigenvalues and corresponding eigenvectors of a real symmetric matrix, while in LAPACK the investigated function is `zheevr`, which calculates a given range of eigenvalues and if required the belonging eigenvectors of a complex hermitian matrix. All functions are in the end of order $O(n^3)$ [7] [16]. Both work with similar algorithms: First, the matrix is transformed to tridiagonal form T via similarity relations which conserve the eigenvalues and the symmetry of the matrix [19]. Afterwards, the eigenvalues are calculated via QR decomposition in GSL or by the `dqds` algorithm in LAPACK, if special eigenvalues are recognized (the `dqds` algorithm is not explained in the following since it does not take more than order $O(n^3)$ and is therefore not characteristic for the complexity of `zheevr`). Tridiagonalization is of order $O(n^3)$ and therefore the major computation time cause. For QR decomposition as well as for tridiagonalization different methods exist: Gram Schmidt orthogonalization, Givens Rotation, but the most common and in the considered libraries used one is the householder transformation [18] [7]. A householder transformation matrix is used to remove a given number of column and/or row entries of a matrix.

Such a matrix has the following form and properties:

$$\begin{aligned}
 H &= \mathbf{1} - 2vv^T, \quad |v| = 1 \\
 H^T &= H \text{ symmetric}, \quad H^T = H^{-1} \text{ orthogonal}
 \end{aligned} \tag{7.8}$$

where the outer product between the vectors v produces a matrix.

Pictorially, the matrix H acting on another vector x results the reflection of it at the axis orthogonal to v .

7.3.1 Tridiagonalization

Tridiagonalization means, that the resulting matrix has entries only on the diagonal and on the upper and lower second diagonal [7]. It is performed to stabilize the following algorithm that computes eigenvalues and speed it up. For the tridiagonalization, column as well as row entries, need to be removed. Therefore Householder matrices acting from both sides on the matrix as a similarity transformation are needed:

$$T = Q^T A Q, \quad Q = \prod_{i=1}^{n-2} H_i \quad (7.9)$$

where H_i are $n-2$ Householder matrices. The algorithm to find the matching Householder matrices and let them act on a $n \times n$ matrix A is:

$k = 1, B = A$

- $s = \sqrt{\sum_{i=k+1}^n b_{ik}^2}$
– if $s=0 \Rightarrow k \rightarrow k+1$, calculate s new
- $v_i = 0 \forall i = 0, \dots, k$
 $v_{k+2} = \sqrt{2}$
 $v_i = \frac{SG \cdot b_{ki}}{2 \cdot v_{k+1} \cdot s} \forall i = k+2, \dots, n$
- $H = \mathbb{1} - 2vv^T$
- $A = H \cdot B \cdot H$
- if $k = n - 2 \Rightarrow A$ is tridiagonal, stop
- $k \rightarrow k+1, B = A$, start again

The complexity is of order $O(n^3)$, because matrix multiplication occurs. If the eigenvectors are of interest later, Q needs to be computed explicitly (and stored) and the exact complexity is $\frac{8n^3}{3}$. Otherwise only the tridiagonal matrix T needs to be stored which is of order $\frac{4n^3}{3}$ [19].

7.3.2 QR decomposition

In a QR decomposition, the matrix is distinguished into an orthogonal matrix Q and an upper triangular R , from which the eigenvalues can be read off. The general process of QR decomposition is described, which can be applied to a tridiagonal matrix. To form a upper triangular matrix R , only the entries lower than the diagonal have to be removed and therefore a multiplication from the left with $n-1$ Householder matrices is sufficient:

$$R = Q^T A, \quad Q = \prod_{i=1}^{n-1} H_i \quad (7.10)$$

$$\Rightarrow A = QR = H_1 \cdot \dots \cdot H_{n-1} \cdot H_{n-1} \cdot \dots \cdot H_1 \cdot A$$

where H_i are the $n-1$ Householder matrices. The algorithm to find the matrices works similar to the tridiagonalization case, but only the lower triangular needs to be removed this time. The dimension of the treated matrix A shrinks in the following algorithm (in every iteration by one), and the entries in the missing dimensions are the already generated numbers in the developing upper triangular matrix. The algorithm for a $n \times n$ matrix A is:

$k=1$, a_1 is the first column of the matrix A

- $\alpha = |a_1| \cdot \text{sgn}(a_{11})$
- $u = a_1 - \alpha \cdot e_1$
- $v = \frac{u}{|u|}$
- $H_k = \mathbb{1}_{n-k+1} - 2vv^T$
- $A_k = H_k \cdot A_{k-1}$
- if $k=n-1 \Rightarrow A$ is 2×2 and R is generated

where H_i are the $n-1$ Householder matrices and e_1 is the first unit vector in the basis of shrinking A . The simplification to tridiagonal form speeds the QR decomposition up, so that the complexity is only $24n^2$ without eigenvectors and $6n^3$ if they need to be computed [19].

7.3.3 LAPACK function: zheevr

The LAPACK function works in a similar way and has a complexity of $O(n^3)$ [16]. It has the advantage, that the user can choose the range of eigenvalues and if eigenvectors should be calculated or not. Additionally, zheevr can handle complex hermitian matrices and not only real symmetric ones, which could be of interest if complex models will be treated in the future.

The idea, that it may be faster than the gsl function arose, because one can calculate single eigenvalues instead of all. The problem is, that the time wasting tridiagonalization is needed anyway [16].

Implementing the LAPACK library in a C++ code is not trivial since LAPACK is written in Fortran. The implementation is described below:

- Download LAPACK libraries to Linux Ubuntu:
 - `sudo apt-get install gfortran`
 - `sudo apt-get install libblas-dev`
 - `sudo apt-get install liblapack-dev`
- Include external functions (written in other languages) in C; write the following in your C-file:


```
#define F_
#ifdef F_
#define _F(s) s##_
#else
#define _F(s) s
#endif
extern"C" {
functiontype _F(functionname) (variabletype variable, ...)
}
```

- Compilation order:
g++ -o programname filename.C -lblas -llapack
- Fortran uses call by reference while C uses call by value. Therefore pointer entries should be transferred to fortran functions

7.4 Run time measurement

To validate the theoretical knowledge about the complexity of the analyzed algorithms, a run time experiment is performed to compare the times practically. The shifted power method, zheevr and gsl_eigen_symm_v are compared. The largest eigenvalues were detected to be smaller than 1000 for various chemical potential and temperature and therefore a safety shift of 5000 was used for the Power method. A shift of 50000 increased the computing time for the largest tested matrix (180) around 1.2%. zheevr was set to calculate only the lowest eigenvalue and no eigenvectors, while the GSL function calculates all eigenvalues and the belonging eigenvectors. The first significant differences began at size 40 matrices.

The following results occurred:

TABLE 7.1: Run times in seconds of various smallest eigenvalue calculators

matrix size	time LAPACK	time power method	time GSL
40	41.666690	41.682130	41.872192
60	166.919073	167.033397	167.578391
90	703.859076	703.469764	706.325420
130	2740.512141	2835.361280	2740.252389
180	10926.52869	10926.612059	10897.650380

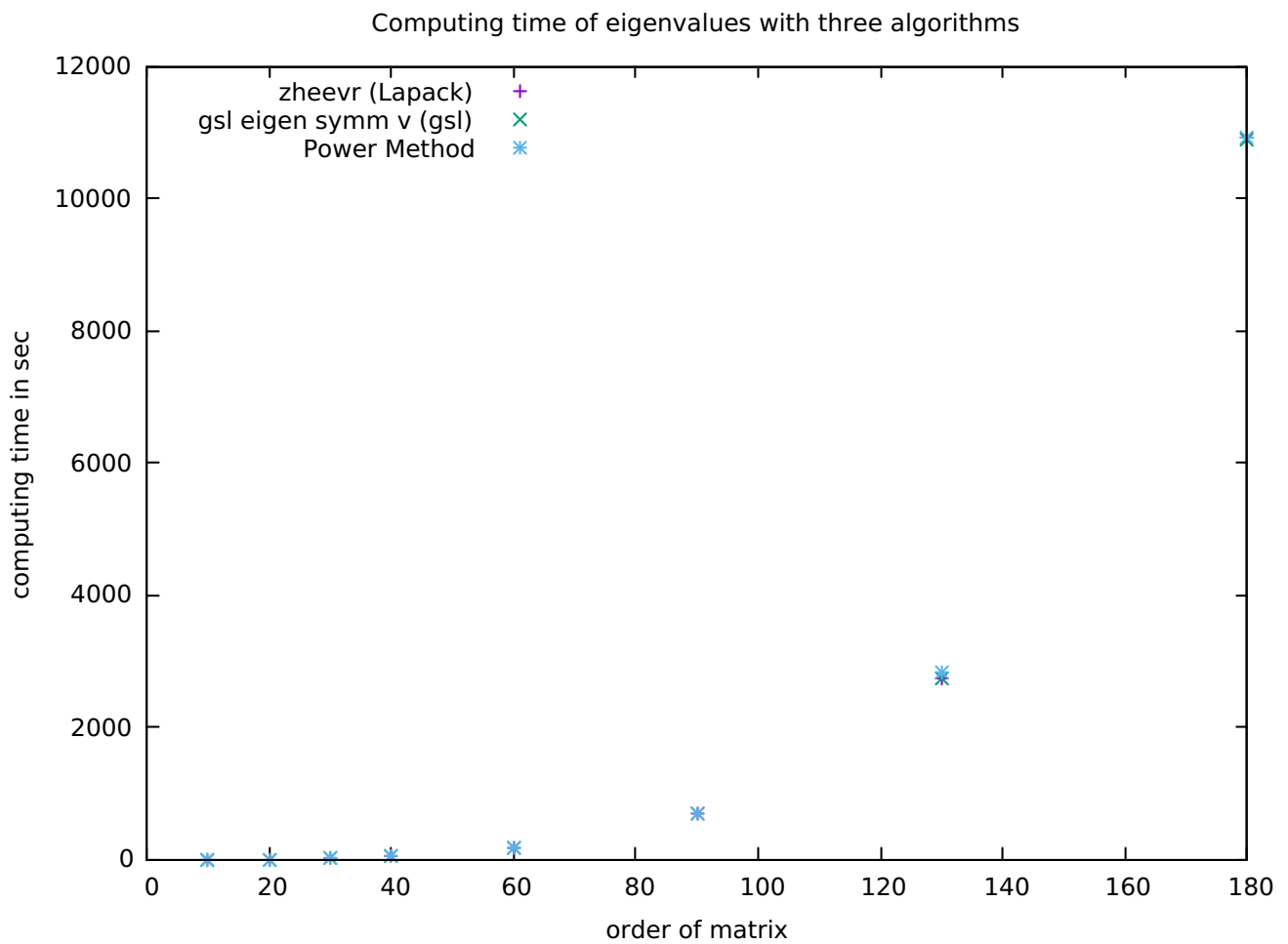


FIGURE 7.1: Computing time plot

Obviously, the times do not differ too much. As expected, zheevr is faster, except for the last calculation, which is surprising. The power method is at least able to compete with the highly developed libraries, but the unpredictability of the run time of an iterative process causes that it is sometimes faster or slower than the other algorithms. Tests with higher order matrices will be needed to make final statements, but none of the algorithms promised a large reduction of computing time yet.

Chapter 8

Conclusion

Summarizing, it can be said, that the major goal: Computing the phase boundaries, of second order transitions by stability analysis is fulfilled and that the developed methods can be applied to other models in a large-N limit. The results of these calculations should only give a first assumption of the phase diagram since only second order phase boundaries can be detected. Additionally, sign changes in the curvature in e.g. zero can appear without a phase transition (pseudo second order) or the curvature can keep its sign while crossing a first order transition. The eigenvector corresponding to the lowest eigenvalue can give a first approximation to the form of the chiral crystal, as long as it points to the global minimum. The goal to speed the slow calculation of eigenvalues up is not fulfilled yet.

8.1 Outlook

One of the first following goals will be to investigate in the purely homogeneous phase in the pseudo 2nd order phase boundary, which shows an unphysical behavior for growing N_T . Still one of the most important aims is finding a way to bypass the slow eigenvalue calculation and a promising way to do so is using the additional translational symmetries of the Hessian matrix, which is a so called Toeplitz matrix. The entries of this class of matrices only depend on the difference between their indices. Fast algorithms seem to exist, to calculate the eigenvalues of symmetric Toeplitz matrices which are only of order $O(n^2)$, but this needs to be studied in detail. Furthermore, the results until now are only approximative expectations. To find the real minimum of an action that depends on a space dependent function, a multidimensional minimization is needed. Various of these algorithms are accessible on GSL, that use the way of steepest descent i.e., the direction given by the negative gradient, to find the minimum. To find a global minimum other strategies are needed, since the algorithm starts anywhere in a multidimensional mountains range and the global minimum is maybe not accessible without crossing a hill. Therefore, an algorithm should also go upwards with a given percentage. One possibility to do so is simulated annealing. The algorithm starts at a given $\vec{\sigma}_i$ and chooses an arbitrary adjacent $\vec{\sigma}_{i+1}$, calculates its value and changes to this point if its value is lower or, if the value is higher, it changes with a given probability.

8.2 Acknowledgements

I would like to thank my supervisor Marc Wagner for a very interesting semester, hours of discussing and helpful explanations. Especially for his code, that I used, like the complete implementation of the homogeneous case and partial implementations of the inhomogeneous one, I want to express my gratitude. Furthermore, I want to thank Dirk Rischke, Florian Divotgey, Niklas Zorbach, Marc Winstel, Laurin Panullo, Noah Stürtz for helpful comments and discussions and GSL, LAPACK for using their libraries.

Bibliography

- [1] P. de Forcrand and U. Wenger, PoS LAT **2006**, 152 (2006) doi:10.22323/1.032.0152 [hep-lat/0610117].
- [2] M. Wagner, Phys. Rev. D **76**, 076002 (2007) doi:10.1103/PhysRevD.76.076002 [arXiv:0704.3023 [hep-lat]].
- [3] O. Schnetz, M. Thies and K. Urlichs, Annals Phys. **314**, 425 (2004) doi:10.1016/j.aop.2004.06.009 [hep-th/0402014].
- [4] PhysRevD.10.3235, title = Dynamical symmetry breaking in asymptotically free field theories, author = Gross, David J. and Neveu, André, journal = Phys. Rev. D, volume = 10, issue = 10, pages = 3235–3253, numpages = 0, year = 1974, month = Nov, publisher = American Physical Society, doi = 10.1103/PhysRevD.10.3235, url = <https://link.aps.org/doi/10.1103/PhysRevD.10.3235>
- [5] CRC-TR 211, <https://th.physik.uni-frankfurt.de/~strongmatter/#Intro>
- [6] M. Wagner, A03 Notes, University of Frankfurt, Unpublished
- [7] Golub and van Loan, Matrix computations 8.3, Third edition, 1996, <http://web.mit.edu/ehliu/Public/sclark/Golub%20G.H.,%20Van%20Loan%20C.F.-%20Matrix%20Computations.pdf>
- [8] D. Rischke, Quantenfeldtheorie 1 & 2, University of Frankfurt, 2018 https://th.physik.uni-frankfurt.de/~drischke/Skript_QFT_I.pdf
- [9] M. Wagner, Fortgeschrittene QFT und QCD, University of Frankfurt, 2015, Unpublished
- [10] M. Wagner, B-Physik und Gittereichtheorie, University of Frankfurt, 2009, https://th.physik.uni-frankfurt.de/~mwagner/talks/B_Physik.pdf
- [11] T. Brauner, Confinement and chiral symmetry breaking in QCD-like theories, University of Frankfurt, 2009, https://www.univie.ac.at/lunch-seminar/talks2009/brauner_0112.pdf
- [12] J. Scheunert, BA: Chirale Symmetrie auf dem Gitter, Implementierung des Overlap-Operators in 1+1 Dimensionen, University of Frankfurt, 2013, https://th.physik.uni-frankfurt.de/~mwagner/theses/BA_Scheunert.pdf
- [13] M. Wagner, Numerische Methoden, University of Frankfurt 2018 https://th.physik.uni-frankfurt.de/~mwagner/teaching/numerical_methods/numerical_methods.pdf
- [14] M. Winstel, BA: Phase diagrams of QCD-inspired models in the large-N limit, University of Frankfurt, Unpublished
- [15] M. Wagner, N. Zorbach, M. Winstel, J. Stoll, Poster: Numerical computation of phase diagrams of QCD inspired models in the large-N limit, University of Frankfurt, 2018 https://th.physik.uni-frankfurt.de/~mwagner/talks/XQCD_2018_poster.pdf
- [16] NAG Library Routine Document F08FRF (ZHEEVR) https://www.nag.co.uk/numeric/fl/nagdoc_fl123/pdf/F08/f08frf.pdf

-
- [17] P. Arbenz, Lecture notes Chapter 2, ETH Zürich, <http://people.inf.ethz.ch/arbenz/ewp/Lnotes/chapter2.pdf>
- [18] Netlib, Eigenvalue problems <https://www.netlib.org/lapack/lug/node70.html>
- [19] P. Arbenz, Lecture Notes Chapter 4, ETH Zürich, <http://people.inf.ethz.ch/arbenz/ewp/Lnotes/chapter4.pdf>
- [20] Netlib, Power Method <http://www.netlib.org/utk/people/JackDongarra/etemplates/node95.html>
- [21] P. Scior, Lattice Simulations of QCD like theories at finite Baryon density, University of Darmstadt, 2016 <http://tuprints.ulb.tu-darmstadt.de/5625/1/main.pdf>
- [22] L. von Smekal, Nucl. Phys. Proc. Suppl. **228**, 179 (2012) doi:10.1016/j.nuclphysbps.2012.06.006 [arXiv:1205.4205 [hep-ph]].
- [23] Analysis 2, Uni Ulm, 2015 https://www.uni-ulm.de/fileadmin/website_uni_ulm/mawi.stukom/baur/WS1516/Ana2/Definitheit.pdf
- [24] University of Montenegro http://www.ucg.ac.me/skladiste/blog_10701/objava_23569/fajlovi/lu.pdf